AUT Journal of Mechanical Engineering

AUT J. Mech. Eng., 10(2) (2026) 211-230
DOI: 10.22060/ajme.2025.24218.6184

Hybrid Nonlinear Model Predictive Control of a Flexible Satellite

Morteza Salehipour[1], Maryam Malekzadeh*[2], Mahdi Mortazavi[1], Mohammad Sayanjali[3]

[1] Department of Aerospace Engineering, University of Isfahan, Isfahan, Iran.
[2] Department of Aerospace Engineering, Sharif University of Technology, Tehran, Iran.
[3] Satellite Systems Institute, Iranian Space research Center, Tehran, Iran.

ABSTRACT: This paper provides a hybrid control strategy for the aim of nullifying the vibration of flexible appendages in satellite structures. These vibrations often occur during the deployment of satellite panels. To maintain performance and ensure attitude stability, a robust control framework is essential. To achieve this, piezoelectric actuators are incorporated into the panels to actively suppress structural vibrations. Lyapunov Nonlinear Model Predictive Control (LNMPC) is introduced in order to guarantee satellite stability and robustness. This algorithm is similar to the Piece-Wise Affine (PWA) method, but the nonlinear dynamics of the system is used instead of linearization. Additionally, Anti-Unwinding Sliding Mode Control is employed into this algorithm and combined with LNMPC to neutralize the vibration actively, furthermore this composite controller assists to control both kinematics and dynamics properly also steering the reaction wheels to zero after every maneuver to save energy in the presence of uncertainty, external disturbance and actuators dynamics considered into the algorithm. Furthermore, close loop stability analysis is provided by utilizing a candidate Lyapunov function.

Review History:
Received: Jun. 03, 2025
Revised: Aug. 18, 2025
Accepted: Oct. 19, 2025
Available Online: Oct. 28, 2025

Keywords:
Hybrid Controller
Flexible Satellite
Nonlinear Model Predictive Control
Anti-Unwinding Sliding Mode Controller
Vibration Suppression
Momentum Management

1- Introduction

Over the past few years, the use of satellites to assist with various tasks has become a common practice in the field of space exploration. However, significant costs are often associated with these missions, which frequently encounter numerous challenges. Once deployed into their predetermined orbits, flexible satellites unfold their solar panels to absorb sunlight and generate electricity. This process can cause vibrations that may disrupt the satellite's attitude. Therefore, designing an appropriate control system is essential to ensure satellite stability.

Lyapunov nonlinear model predictive control is a robust control strategy that is widely used across different industries. It employs a cost function to optimize the algorithm and guide the system toward a steady state. Two common optimization methods are the active set method and sequential quadratic programming. In this paper, we have chosen the active set method due to its ability to solve quadratic programming problems with high accuracy and speed. Active set method usually are used in linear applications but in this study it's correspondence with nonlinear systems are discussed[1].

Anti-unwinding sliding mode control(AUSMC) is employed additionally to assurance kinematics convergence. This issue has been recognized by many scientists and researchers, a linear model predictive control and a terminal sliding mode controller are combined to passive suppress the satellite's vibrations in and enhance satellite stability in the presence of actuator faults[2].

Hybrid controller involving model predictive control and feedback linearization are designed. This combination has ability to both control the attitude and angular velocity of the reaction wheels[3].

MPC used due to station keeping and momentum management of a low-thrust satellite. MPC is scheduled to maintain the satellite in a tight latitude and longitude frame[4].

An extended model predictive control (EMPC) is employed in order to keep the satellite in a nadir direction in the presence of actuator faults. This MPC algorithm is similar to the linear model and it needs dynamics model linearization and Hildreth method to handling the constraints[5].

MPC algorithm named multi-horizon multi-model predictive(MHMM-PC) control is discussed.it used a quadratic cost function and sequential quadratic programming (SQP) method to optimize the algorithm due to stabilize a electromagnetic tethered satellite[6].

MPC and LQG (Linear Quadratic Gaussian) are combined for the purpose of the control the satellite attitude and improve the accuracy during docking and refueling. One of the main

*Corresponding author's email: m.malekzadeh@eng.ui.ac.ir

challenges is fuel sloshing disturbance, and it can disrupt the satellite attitude to prevent this, these to controllers are merged to optimize and enhance the performance of the satellite. The linear MPC is used in this paper [7].

For the aim of control the high thrust in a cube sat with solid thruster a piece-wise affine model predictive control (PWA-MPC) is proposed. Solid thruster usually have a large eccentric torque and it can lead to rapid attitude maneuvering so MPC for the reason that it can frequently optimize the system can improve the cube sate thruster torque in an accuracy way is chosen and in this paper linear model is used[8].

A new NMPC algorithm named multivariate radial basis function-based autoregressive model which uses sequential quadratic programming(SQP) to optimize the system for the propose of satellite attitude control[9].

All these researches are compared to this work, in this study flexible satellite nonlinear dynamics are incorporated into a Toeplitz matrix, and by optimizing it by active-set method the optimal control signal is yielded. Conventionally, the active-set method utilizes when inequality active constraints are in the problem, so in this work it is assumed that, if high maneuver is needed so satellite consumes high control effort and it is lead to active constraints in every optimal solution, moreover active -set method is able to be faster than SQP. Another problem is to steer the actuators to zero and ensure satellite stability every maneuvering in the presence of uncertainty, external disturbance and actuators dynamics, steering reaction wheels to zero will assist to save more energy and use it for the next maneuver.

The contributions of this paper are listed below

Forming a Toeplitz matrix containing the nonlinear equations of a flexible satellite, also it is optimized by active-set algorithm which is faster and more accurate that SQP

Merging LNMPC and AUSMC in order to neutralize the satellite vibration in active mode

Focusing on satellite momentum management and the reaction wheels will be stop after maneuvering is accomplished.

Considering Modified Rodriguez Parameters (MRPs) as satellite kinematics equation and analysis hybrid controller performance in the presence of uncertainty, external torques and actuator dynamics.

In this paper, section 2 provides the 3DOF flexible satellite attitude dynamics, section 3 outlines about satellite control system design, section 4 is about the closed loop stability analysis, section 5 is illustrated the simulation diagrams and finally section 6 is a conclusion about our work.

2- Flexible Satellite Dynamics and Kinematics

Flexible spacecraft kinematics and dynamics equations are given.[10],[11]. Dynamic equations are represented by equations (1) and (2), where $\boldsymbol{\omega} \in \boldsymbol{R}^3$ denotes the angular velocity matrix, $\boldsymbol{J} \in \boldsymbol{R}^{3\times3}$ is the positive definite symmetric matrix related to the momentum of inertia of the satellite. $\boldsymbol{\delta} \in \boldsymbol{R}^{3\times n}$ The matrix represents the coupling between the rigid hub and the flexible appendages. $\boldsymbol{\eta} \in \boldsymbol{R}^n$ The vector signifies the modal coordinates related to the main body, and $\boldsymbol{u} \in \boldsymbol{R}^3$, $\boldsymbol{d} \in \boldsymbol{R}^3$ characterize the control effort vector and external disturbances, respectively. Additionally, $\boldsymbol{C} = 2\xi\Omega_n \in \boldsymbol{R}^{n\times n}$ is the damping diagonal matrix, and $\boldsymbol{K} = \Omega_n{}^2 \in \boldsymbol{R}^{3\times n}$ is the stiffness diagonal matrix, $\boldsymbol{\delta}_p \in \boldsymbol{R}^{3\times3}$ is the matrix indicates a coupling matrix related to the flexible. Furthermore, $\boldsymbol{u}_p \in \boldsymbol{R}^3$ represents the piezoelectric control input acting on the flexible appendages. Equation (3) denotes the angular velocity skew-symmetric matrix, which is utilized in equation (1).

$$\dot{\boldsymbol{\omega}}\boldsymbol{J} + \boldsymbol{\omega}^{\times}\boldsymbol{J}\boldsymbol{\omega} + \boldsymbol{\delta}\ddot{\boldsymbol{\eta}} = \boldsymbol{u} + \boldsymbol{d} \tag{1}$$

$$\ddot{\boldsymbol{\eta}} + \boldsymbol{C}\dot{\boldsymbol{\eta}} + \boldsymbol{K}\boldsymbol{\eta} = -\boldsymbol{\eta}^T\boldsymbol{\omega} - \boldsymbol{\delta}_p\boldsymbol{u}_p \tag{2}$$

$$\boldsymbol{\omega}^{\times} = \begin{bmatrix} 0 & -\omega_3 & \omega_2 \\ \omega_3 & 0 & -\omega_1 \\ -\omega_2 & \omega_1 & 0 \end{bmatrix} \tag{3}$$

Equations(4) and (5) are represented piezoelectric actuator voltage input computation.

$$\boldsymbol{y} = \boldsymbol{p}\dot{\boldsymbol{\eta}} \tag{4}$$

$$\boldsymbol{u}_p = \boldsymbol{\delta}^T\boldsymbol{p} \tag{5}$$

Equation (6) is used due to investigation the complexity of the model and considering the effect of the panels' vibration into the equation and to improve accuracy, so in the whole of this paper this equation is utilized in the nonlinear equation.

$$\boldsymbol{J} = \boldsymbol{J}_1 - \boldsymbol{\delta}^T\boldsymbol{\delta} \tag{6}$$

Equations (7) and (8) are related to the Euler angles of the satellite $\Theta = [\phi \quad \theta \quad \psi]$ and Fig.1 is depicted a schematic of a flexible satellite which is extracted from [12].

$$\dot{\Theta} = \boldsymbol{R}\boldsymbol{\omega} \tag{7}$$

$$\boldsymbol{R}^{-1} = \begin{bmatrix} 1 & 0 & -\sin\theta \\ 0 & \cos\phi & \sin\phi\cos\theta \\ 0 & -\sin\phi & \cos\phi\cos\theta \end{bmatrix} \tag{8}$$

Equation (9) indicates the kinematic equation, where $\boldsymbol{\sigma} \in \boldsymbol{R}^3$ is the vector related to the Rodriguez parameters.

Fig. 1. Flexible satellite structure model.

$\boldsymbol{I} \in \boldsymbol{R}^{3\times3}$ is the identity matrix.

$$\dot{\boldsymbol{\sigma}} = \frac{1}{4}\{(1-\boldsymbol{\sigma}^T\boldsymbol{\sigma})\boldsymbol{I} + 2\boldsymbol{\sigma}^{\times} + 2\boldsymbol{\sigma}\boldsymbol{\sigma}^T\}\boldsymbol{\omega} \tag{9}$$

2- 1- Actuators Dynamics

In this subsection, actuators dynamics are investigated inspired by [13]. Generally the reaction wheels are DC motors that are mounted in the satellite and can rotate any direction, these actuators should stop after any maneuver, it is for prevent actuators to be saturated or failed. Equation(10) is the differential equation for the armature of the DC motor circuits.

$$\boldsymbol{L_a}\frac{\boldsymbol{di_a}}{\boldsymbol{dt}} + \boldsymbol{R_a i_a} + \boldsymbol{K_b}\boldsymbol{\Omega}_{(i)} = \boldsymbol{e_a} \tag{10}$$

$\boldsymbol{R_a}$ is the armature, $\boldsymbol{L_a}$ denotes the armature inductance, $\boldsymbol{K_b}$ indicates the back emf constant, $\boldsymbol{\Omega}$ is the angular velocity of the motor, $\boldsymbol{i_a}$ is the armature current and $\boldsymbol{e_a}$ denotes the applied armature voltage.

$$\boldsymbol{e_a} = \boldsymbol{K_b}\frac{\boldsymbol{d\theta}}{\boldsymbol{dt}} \tag{11}$$

$\boldsymbol{\theta}$ signifies the angular displacement of the motor shaft and the $\boldsymbol{u_r}$ produced by motors, equation(12) denotes the torques produced by actuators motors and $\boldsymbol{K_m}$ is the motor torque constant.

$$\boldsymbol{u_{r(i)}} = \boldsymbol{K_m i_a} \tag{12}$$

In equation (13), $\boldsymbol{b}$ is the viscous coefficient of the motors.

$$\boldsymbol{J_{r(i)}}\dot{\boldsymbol{\Omega}}_{(i)} + \boldsymbol{b}\boldsymbol{\Omega}_{(i)} = \boldsymbol{u_{r(i)}} = \boldsymbol{K_m i_a}, \boldsymbol{i} = 1,2,3 \tag{13}$$

Equations (14) and (15), $\boldsymbol{K_t}$ and $\boldsymbol{T_m}$ are the motor gain constant and motor time constant respectively.

$$\boldsymbol{K_t} = \frac{\boldsymbol{K_m}}{\boldsymbol{R_a b} + \boldsymbol{K_m K_b}} \tag{14}$$

$$\boldsymbol{T_m} = \boldsymbol{R_a J_r} \times (\boldsymbol{R_a b} + \boldsymbol{K_m K_b}) \tag{15}$$

$$\boldsymbol{J_{r(i)}}\dot{\boldsymbol{\Omega}}_{(i)} + \frac{\boldsymbol{I_{\omega(i)}}}{\boldsymbol{T_m}}\boldsymbol{\Omega}_{(i)} = \boldsymbol{I_{\omega(i)}}\frac{\boldsymbol{K_t}}{\boldsymbol{T_m}}\boldsymbol{e_a} \tag{16}$$

$$\begin{aligned}&(\boldsymbol{J} - \boldsymbol{J_r})\dot{\boldsymbol{\omega}} = -\boldsymbol{\omega}\times(\boldsymbol{J\omega} + \boldsymbol{J_r}\boldsymbol{\Omega})\\ &-(\boldsymbol{J_r}\bar{\boldsymbol{K}}_{\boldsymbol{t}}\boldsymbol{T_m}^{-1}\boldsymbol{e_a} - \boldsymbol{J_r}\boldsymbol{T_m}^{-1}(\boldsymbol{\omega}+\boldsymbol{\Omega})) + \bar{\boldsymbol{T}}_{\boldsymbol{d}}\end{aligned} \tag{17}$$

$$\ddot{\boldsymbol{\eta}} + \boldsymbol{C}\dot{\boldsymbol{\eta}} + \boldsymbol{K}\boldsymbol{\eta} + \boldsymbol{\delta}\dot{\boldsymbol{\omega}} = -\boldsymbol{\delta_p}\boldsymbol{u_p} \tag{18}$$

Equations (17) and (18) outline the nonlinear dynamics of the flexible satellite in the presence of actuators dynamics. In equation (16) $\boldsymbol{e_a}$ is considered as control input.

3- Attitude Control System Design

This section focuses on controller design. Fig.2 illustrates the configuration of the proposed hybrid controller. This diagram shows the integration of the Anti-Unwinding Sliding Mode Controller (AUSMC) with the Lyapunov Nonlinear Model Predictive Controller (LNMPC). In this block diagram, an arbitrary input is applied to the LNMPC, and the desired output is fed back to the input in order to minimize

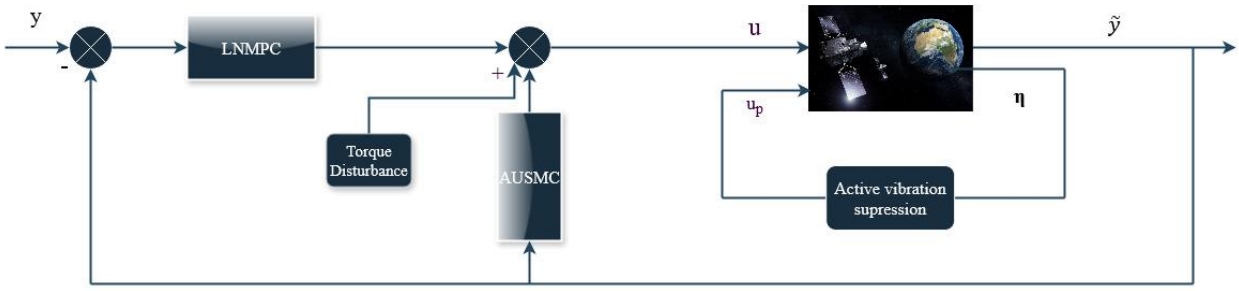

Fig. 2. Block diagram of the hybrid controller.

the error to zero. Sections 3 is dedicated to the design of the controllers.

3- 1- Lyapunov Nonlinear Model Predictive Control Design

Lyapunov nonlinear model predictive control equations are derived according to [14]. Totally model predictive control is based on optimal control so for solving the optimal control problem we need a cost function. This function which is shown in(19), it optimizes dynamic system error in a finite prediction horizon and optimal control derivative vector will be computed, and first element of the vector is applied to the system. the predicted outputs are $\tilde{y} = \left[\tilde{\sigma} \quad \tilde{\omega} \quad \tilde{h}_{\omega}\right]$. $\boldsymbol{Q}$ and $\boldsymbol{R}$ are the weighting matrices related to the trajectory error and control effort variation respectively. In NMPC by minimizing the quadratic cost function, the predicted output $\tilde{y}$ can be converge to it's set point $\boldsymbol{y}$ faster and smoother.

$$\min_{\Delta u} J = \sum_{j=N}^{N_p} Q_j \left((\tilde{y}(k+j \mid K) - y(k+j \mid k)\right)^2 + \sum_{i=0}^{N_u-1} R_i \Delta u(k+i \mid k)^2 \tag{19}$$

As mentioned previously, one of the advantages of the MPC is to take constraints into account. Equations (20), (21), and (22) discuss these constraint limitations. In this paper, the control effort u and variations in control effort Δu are the system's constraints.

$$u_{\min} \le u(k+i \mid k) \le u_{\max}. \tag{20}$$

$$u_{\min} \le u(k+i \mid k) \le u_{\max} \tag{21}$$

$$\Delta u_{\min} \le \Delta u(k+i \mid k) \le \Delta u_{\max} \tag{22}$$

In Equation (23), the term $\tilde{Y}$ represents the estimated output of the system. This term is determined by solving the optimization problem outlined in Equation (26). F The steady states relevant to this problem G are expressed here as well. The Toeplitz matrix, as described in Equation (29), is used to analyze the differences between past and future behaviors of the system over the finite prediction horizon N_p concerning variations in control effort.

$$\tilde{Y} = F + G\Delta U \tag{23}$$

$$\tilde{Y} = \begin{bmatrix} \tilde{y}(k+1 \mid k) \\ \tilde{y}(k+2 \mid k) \\ \vdots \\ \tilde{y}(k+N_p \mid k) \end{bmatrix}, \Delta U = \begin{bmatrix} \Delta u(k \mid k) \\ \Delta u(k+1 \mid k) \\ \vdots \\ \Delta u(k+N_c-1 \mid k) \end{bmatrix} \tag{24}$$

$$F = \tilde{Y}_{N_p \times 1} \tag{25}$$

$$J = \frac{1}{2}\Delta U^T \phi \Delta U + \theta^T \Delta U \tag{26}$$

$$\phi = 2(G^T Q G + R) \tag{27}$$

$$\theta = G^T Q (F - Y) \tag{28}$$

$$G = \begin{bmatrix} \frac{\partial \tilde{y}(k+1)}{\partial \Delta u(k)} & 0 & \cdots & 0 \\ \frac{\partial \tilde{y}(k+2)}{\partial \Delta u(k)} & \frac{\partial \tilde{y}(k+2)}{\partial \Delta u(k+1)} & \cdots & 0 \\ \vdots & \vdots & \ddots & \vdots \\ \frac{\partial \tilde{y}(k+N_p)}{\partial \Delta u(k)} & \frac{\partial \tilde{y}(k+N_p)}{\partial \Delta u(k+1)} & \cdots & \frac{\partial \tilde{y}(k+N_p)}{\partial \Delta u(k+N_u-1)} \end{bmatrix} \tag{29}$$

Equations (30) and (31) are denoted the predicted output

and control effort variations.

$$\partial\tilde{y} = \tilde{y}(k) - \tilde{y}(k-1) \tag{30}$$

$$\partial\Delta u = \Delta u(k) - \Delta u(k-1) \tag{31}$$

The equations above have been used to solve the quadratic cost function in (26), and the optimization was performed using the active-set method in MATLAB. One of the advantages of this algorithm is its use of a candidate Lyapunov function in the matrix G, which allows for stability analysis to be integrated into the algorithm. It assists to enhance the robustness of the controller. It is important to note that matrix $\boldsymbol{G}$ is the forced response and the matrix $\boldsymbol{F}$ is the free response.

3- 2- Anti-Unwinding Sliding Mode Control Design

In this section anti-unwinding sliding mode controller is presented. This nonlinear controller is used due to guarantee kinematics asymptotic stability[15]. Sliding mode is a nonlinear controller which employs a sliding surface to stabilize the steady states. One the common problems of sliding mode controller is chattering phenomenon. Chattering is a harmful event which occurs in control effort signal and it could damage actuators.to prevent it, some kind of sliding mode controller have been developed by researchers and it can be seen in many papers. Briefly, unwinding is a phenomenon that satellite to reach it's desired attitude from an arbitrary point needs to rotate more than π so anti-unwinding method makes satellite to keep this rotation less than π. at first it is need to design a sliding surface S and steady states should be in it. In equation (32) predicted angular velocity $\tilde{\omega}$ and Modified Rodriguez parameters $\tilde{\sigma}$ is put into the sliding surface. Term λ is a positive weighting constant and assume to be 0.3 due to control the kinematics.

$$\boldsymbol{S} = \tilde{\omega} + \lambda\tilde{\sigma} \tag{32}$$

Equation (33) depicted the AUSMC control law (u). u_{eq}, u_n are obtained by solving the (34) to (38).in nominal control law (u_n), γ_1 is a positive constant and chosen to be 0.1, γ_2 is acquired by (36).

$$\left\{\begin{array}{c} \boldsymbol{u} = \boldsymbol{u}_{eq} + \boldsymbol{u}_n \\ \boldsymbol{u}_{eq} = \boldsymbol{\omega}^{\times}\boldsymbol{J}\tilde{\omega} - \lambda\boldsymbol{J}\boldsymbol{M}(\tilde{\sigma})\tilde{\omega} \\ \boldsymbol{u}_n = -(\gamma_1 + \gamma_2(t))\boldsymbol{J}\boldsymbol{f}(\boldsymbol{s}) \\ \boldsymbol{s} = \tilde{\omega} + \lambda\tilde{\sigma} \end{array}\right\} \tag{33}$$

$$\boldsymbol{M}(\tilde{\sigma}) = \frac{1}{4}[(1 - \|\tilde{\sigma}\|^2)\boldsymbol{I}_3 + 2\tilde{\sigma}^{\times} + 2\tilde{\sigma}\tilde{\sigma}^T] \tag{34}$$

$$\sigma_e^{\times} = \begin{bmatrix} 0 & -\sigma_3 & \sigma_2 \\ \sigma_3 & 0 & -\sigma_1 \\ -\sigma_2 & \sigma_1 & 0 \end{bmatrix} \tag{35}$$

$$\gamma_2(t) = \lambda|\dot{g}| \tag{36}$$

The following relations are presented to define the boundary conditions, and equation (38) is a positive-valued function. The term ε is a small positive value, and as it approaches zero, it improves anti-unwinding performance.

$$\boldsymbol{g} = \left\{\begin{array}{l} \|\tilde{\sigma}\|, \arctan\sqrt{\tilde{\sigma}^T\tilde{\sigma}} \le \dfrac{\pi}{4} \\ -\|\tilde{\sigma}^s\|, \arctan\sqrt{\tilde{\sigma}^T\tilde{\sigma}} \le \dfrac{\pi}{4} \end{array}\right\} \tag{37}$$

$$\boldsymbol{f}(\boldsymbol{s}) = \left\{\begin{array}{l} \dfrac{\boldsymbol{s}}{\|\boldsymbol{s}\|}, \boldsymbol{if}\ \|\boldsymbol{s}\| \succ \varepsilon \\ \dfrac{\boldsymbol{s}}{\varepsilon}, \boldsymbol{if}\ \|\boldsymbol{s}\| \le \varepsilon \end{array}\right\} \tag{38}$$

The AUSMC algorithm is derived from the equations above and will help ensure that kinematics converges to zero while making controller signals as smooth as possible.

4- Stability Analysis

In this section the closed loop stability is proved by a candidate Lyapunov function. In this proof the candidate Lyapunov function is based on sliding surface in equation (32)

Proof:

The candidate Lyapunov function is given as follows

$$\boldsymbol{V} = \frac{1}{2}\boldsymbol{S}^T\boldsymbol{S} \tag{39}$$

By taking a time derivative the equation (39) is yielded

$$\dot{\boldsymbol{V}}(t) = \boldsymbol{S}^T\dot{\boldsymbol{S}} \tag{40}$$

By substituting the equation (33) into the equation(40), equations(41) and (42) are obtained respectively.

$$\dot{V}(t) = S^T (J^{-1}(-\omega^{\times} J\tilde{\omega} - \delta\ddot{\eta} + u + d) + \lambda\dot{\tilde{\sigma}}) \tag{41}$$

$$\dot{V}(t) = -S^T (J^{-1}(u_n - \lambda J\dot{\tilde{\sigma}} + d) + \lambda\dot{\tilde{\sigma}}) = -S^T (J^{-1}((\gamma_1 + \gamma_2(t))Jf(s)) \tag{42}$$

$$\dot{V}(t) \le -\gamma_1 \|S\| - \gamma_2(t)\|S\| \le -\gamma_2(t)\|S\| \tag{43}$$

So in equation (43), the $V(t) \succ, \dot{V}(t) \le 0$ are achieved and the closed loop system is asymptotically stable.

5- Simulation and Validation

This section presents the results of computer simulations conducted using MATLAB software. We compare the performance of the proposed hybrid controller in actively suppressing vibrations in flexible appendages, all the simulations have done under uncertainty and external disturbance. This comparison aims to evaluate its superiority over the algorithm's performance. This section is divided into two subsections, in subsection 5.1 tuned controller gains which are obtained by trial and error are discussed and subsection 5.2 is related to the computer simulations. In all the simulations in the subsection 5.2 external disturbance and 20 % of the flexible satellite moment of inertia as uncertainty are employed. Furthermore, the Matrix damping is considered as $C = 0$ to analyze the hybrid controller ability in order to neutralize the satellite vibration.

5- 1- Gain Tuning

To ensure the expected performance of the designed controller, the controller's gain must be adjusted rigorously. All performance parameters, including settling time, overshoot/undershoot, steady-state error, prediction horizon, and control horizon, should be considered. As mentioned in section 2, the prediction and control horizons are assumed $N = 10$ to be set, and the controller's gains Q, R are adjusted as $Q = diag(1500,1500,1500)$ $R = diag(10,10,10)$ respectively. The gains for the anti-unwinding sliding mode controller discussed in section 3 are tuned as follows. $\lambda = 0.3$ $\gamma_1 = 0.1$ $\varepsilon = 0.001$ The simulation time is $t = 100s$ set, and the sampling period time step is also specified $t_s = 0.01$. The parameters related to the appendage's vibration and piezoelectric actuators are adjusted $\Omega = diag(0.7681,1.1038,1.8733)$ $P = diag(0.2,0.2,0.2)$ to account for the vibration frequency and the positive definite matrix associated with the piezoelectric actuators, respectively.

5- 2- Simulation Results

To enhance the clarity of the tracking performance and robustness of the controller, the diagrams below are provided. These graphs are generated based on specific initial conditions that mentioned in table 1.To introduce uncertainty into the algorithm, it is assumed that 20 percent of the inertial matrix for the body frame of the flexible satellite is affected. Parameters ϕ, θ, ψ denote the Euler angles, ω is the flexible satellite angular velocity, η is the vibration displacement and it is related to the flexible appendage and σ is the Rodriguez Parameters related to the kinematics equation. It is supposed that the satellite reach the set point y from the given numerical conditions.

Table.2 represents the values of actuators parameters and it is based on actuators motors specifications.

LNMPC is unable to nullify vibration with low frequency, so it is merged AUSCM to tackle this problem. if LNMPC perform as a lowpass filter and just able to neutralize the high frequency the satellite attitude would be interrupted, Fig.2 and Fig.3 are bode diagrams and are given to prove this claim.

The satellite's inertia matrix, coupling matrix, and coupling matrix related to the flexible part are expressed as follows:

Table 1. Initial Conditions.

Number	Parameter	Initial Conditions
1	ϕ, θ, ψ	$[10^\circ \quad -20^\circ \quad 100^\circ]^T$
2	ω	$[0 \quad 0 \quad 0]^T$
3	η	$[0 \quad 0 \quad 0]^T$
4	σ	$[1.5 \quad -0.5 \quad 0.3]^T$
5	u_{max}	10

Table 2. Actuators specifications.

Number	Parameter	Value
1	$R_a(ohm)$	1
2	K_b	0.0005
3	$K_m(\frac{Mm}{A})$	0.2
4	$b(\frac{N.m}{rad.s})$	1.21×10^{-3}

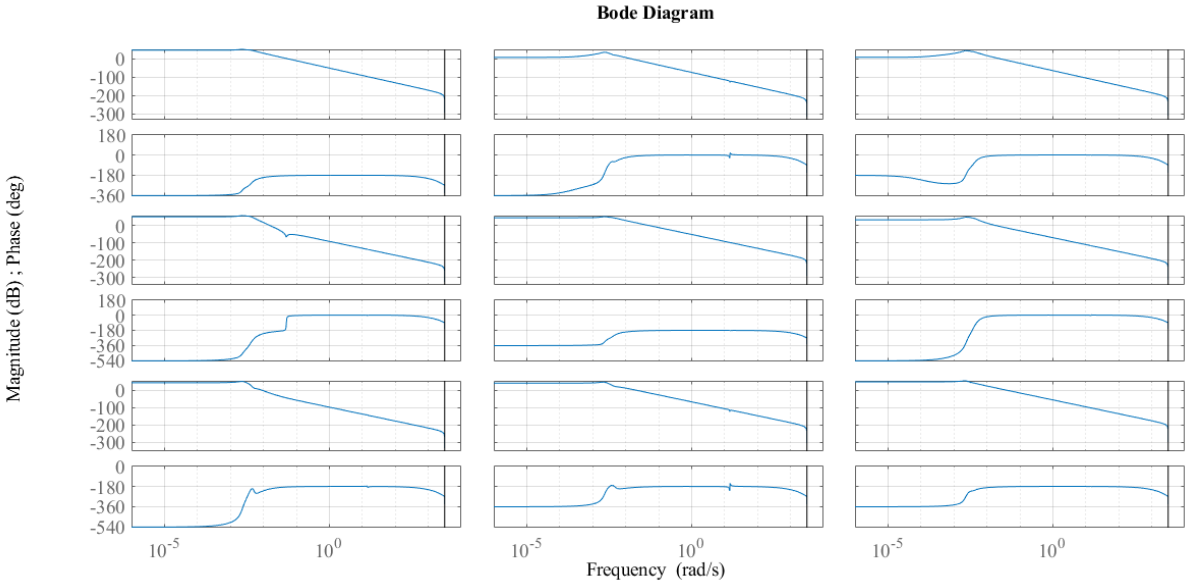

Fig. 3. Bode diagram during vibration suppression using the LNMPC.

$$J=\begin{bmatrix}420.8 & 3.6 & -4.2\\ 3.6 & 410.6 & 9.4\\ -4.2 & 9.4 & 690.7\end{bmatrix} \quad (44)$$

$$\delta=\begin{bmatrix}2.62 & 0.007 & -0.003\\ -0.001 & 0.124 & -2.73\\ -0.001 & 0.437 & -0.051\end{bmatrix} \quad (45)$$

$$\delta_p=\begin{bmatrix}70.26 & -4.23 & 2.34\\ 4.80 & 31.93 & 1.24\\ -1.05 & 2.55 & 29.84\end{bmatrix} \quad (46)$$

By assuming that flexible satellite is placed 500 Km far from the earth surface the external disturbance that is employed to its actuators is[16].

$$d=2\times\begin{bmatrix}\cos(\omega_0 t)+1\\ \cos(\omega_0 t)+\sin(\omega_0 t)\\ \sin(\omega_0 t)+1\end{bmatrix} \quad (47)$$

Where ω_0 is the orbital angular velocity and it is considered as 0.0011 rad/s and the amplitude of the disturbance is 2.

Fig.3 illustrates the bode diagram related to LNMPC active vibration suppression. We have $6\times3=18$ graphs related to 3 inputs and 6 outputs (Euler angles an angular velocities). According to the diagram as frequency increases, the slope of the diagram converges to $-\infty$ it means that the controller is nullifying the high frequency and just pass the low frequency. In Fig.4 exactly the opposite happens, in low

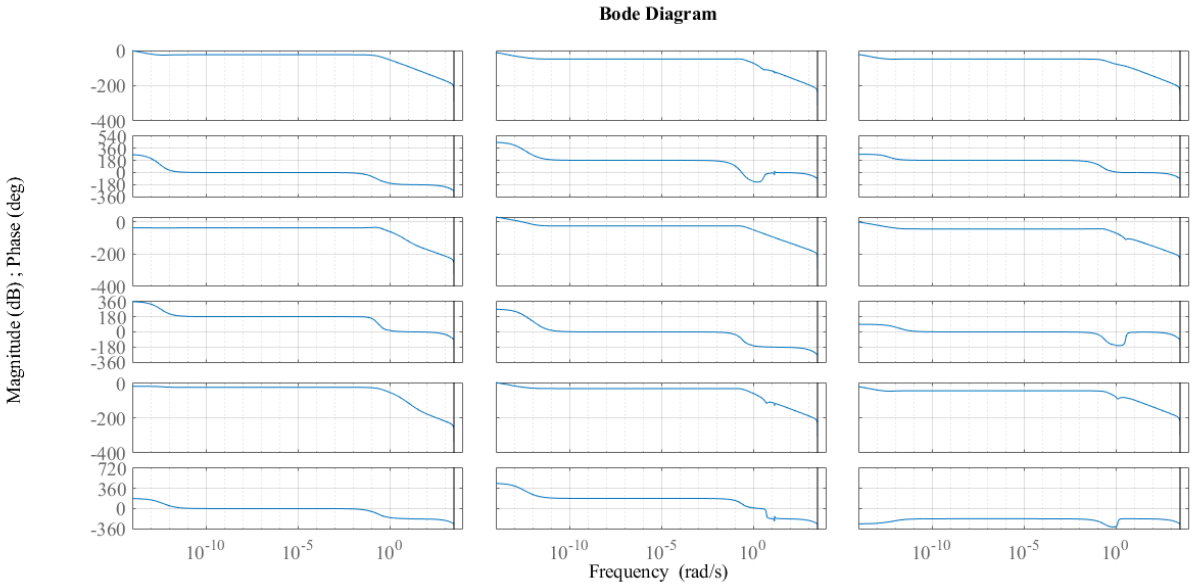

Fig. 4. Bode diagram during vibration suppression using the Hybrid Controller.

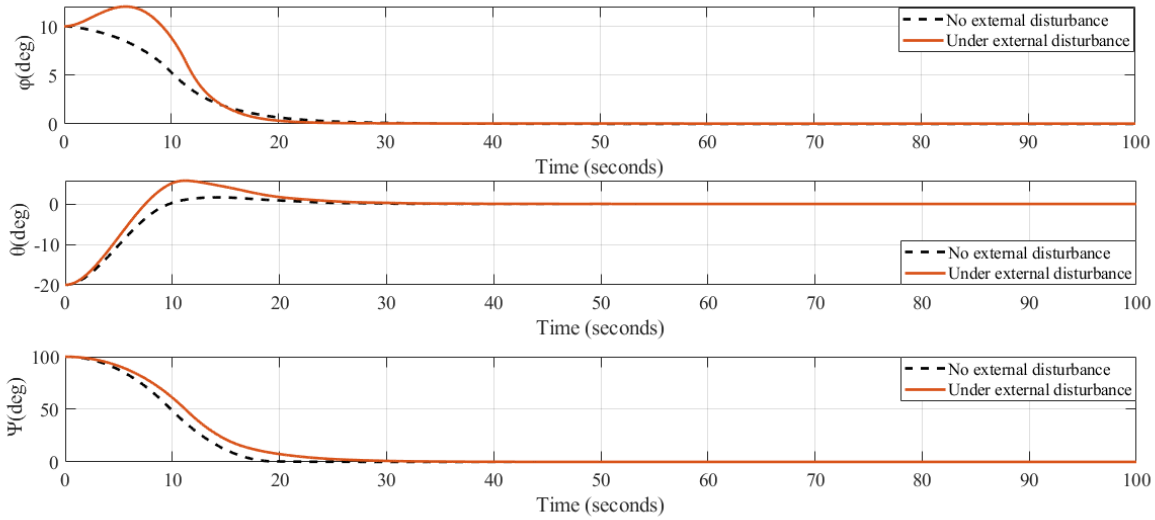

Fig. 5. Flexible satellite Euler angles (ϕ, θ, ψ).

frequency, the frequency that is given in subsection 5.1 the slope remains in negative side or near zero and it is declared that the hybrid controller is nullifying the vibration with low frequency as well.

In the rest of the paper, the figures related to the computer simulations are given. In all simulations the behavior of the composite controller during entering disturbance into the actuators are analyzed. Fig.5 is the satellite Euler angles which are reached to the set point from the arbitrary conditions. Fig.6 is the control effort signals related to all three reaction wheels, Fig.7 is the Rodriguez parameters, Fig.8 is the flexible appendage's vibration displacements, Fig.9 is flexible appendage's vibration velocities, Fig.10 is satellite angular momentums and they are properly steered to zero after maneuver.Fig.11 is the satellite angular velocities, Fig.12 is the sliding surfaces and they are converged to zero as well, Fig.13 is the piezoelectric control input voltage and Fig.14 is the reaction wheels motors angular velocities and they are similar to reaction wheels angular momentum converged to zero. It is essential to stop actuators after each

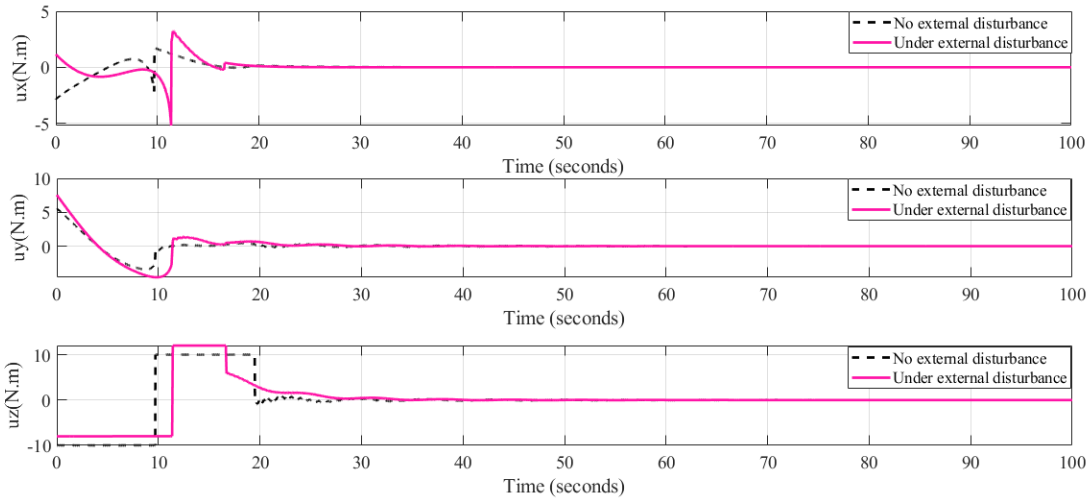

Fig. 6. Control effort signals (u_x, u_y, u_z).

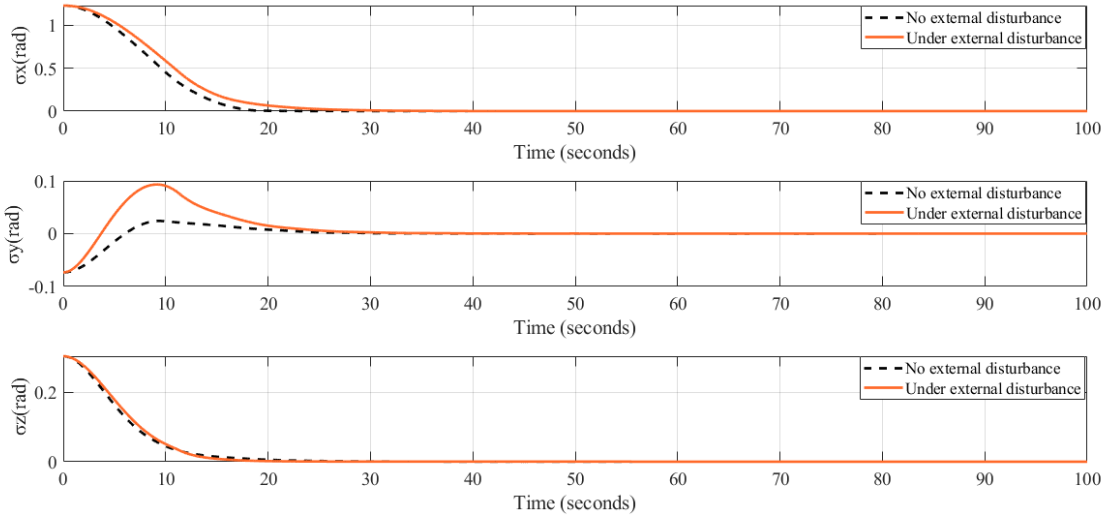

Fig. 7. Modified Rodriguez Parameters ($\sigma_x, \sigma_y, \sigma_z$).

maneuver to prevent over consuming and save energy for the next maneuver.

Table 3. discussed about the behavior of the system after employing external disturbance. The Euler angels and Tip deflection settling times are raised, but it is not a quite different and it is a reason that the hybrid controller is robust enough to handle disturbance with high amplitude. The main reason that this controller is considered as a robust NMPC is the corresponding Toeplitz matrix that contains the nonlinear dynamics of the flexible satellite so it is able to deal with uncertainty and disturbance properly.

Fig.15 depicts the Euler angles error signals comparison in two different states, with and without employing external disturbance. Equation (48) is the Euler angles error and equation(49) gives the convergent rate.

In equation (48) the error of the Euler angles is denoted, where $\Theta = [\phi \quad \theta \quad \psi]$.

$$error = \|\Theta\| \tag{48}$$

$$convergence\_rate = \frac{\partial e}{\partial t} = \dot{e} \tag{49}$$

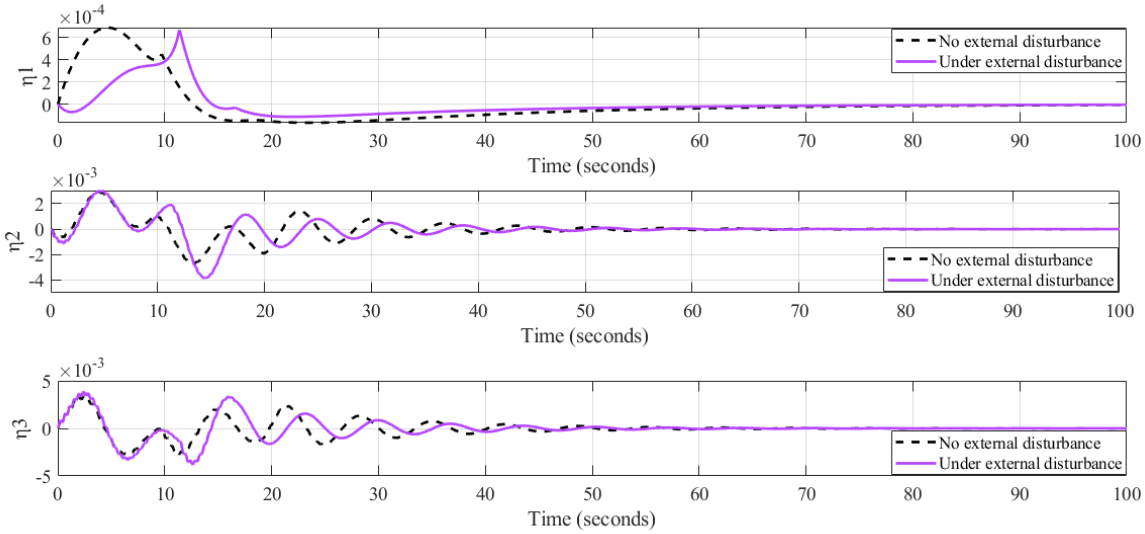

Fig. 8. Vibration displacements (η_1, η_2, η_3).

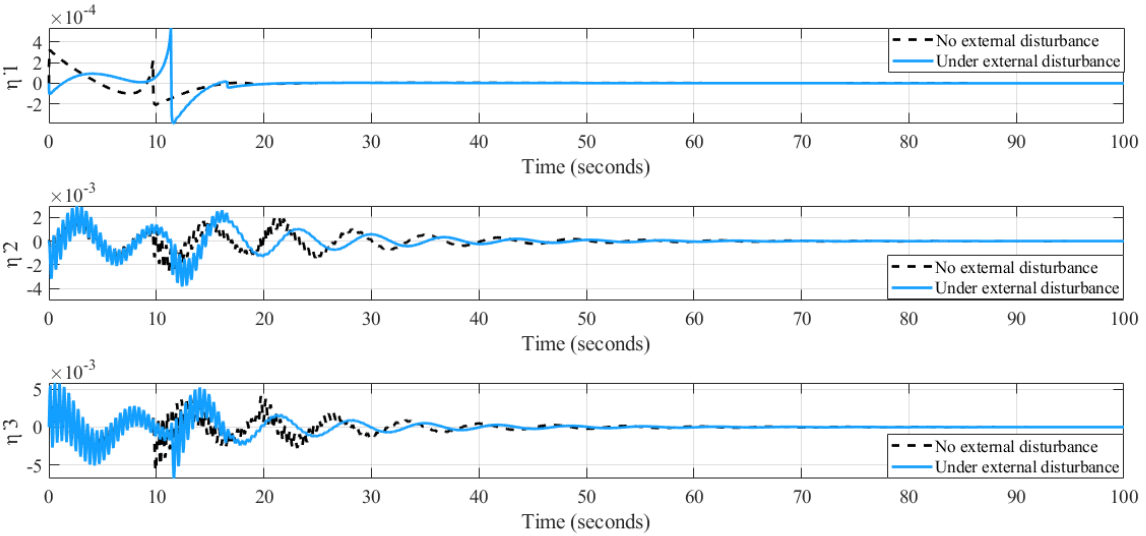

Fig. 9. Vibration velocities ($\dot{\eta}_1, \dot{\eta}_2, \dot{\eta}_3$).

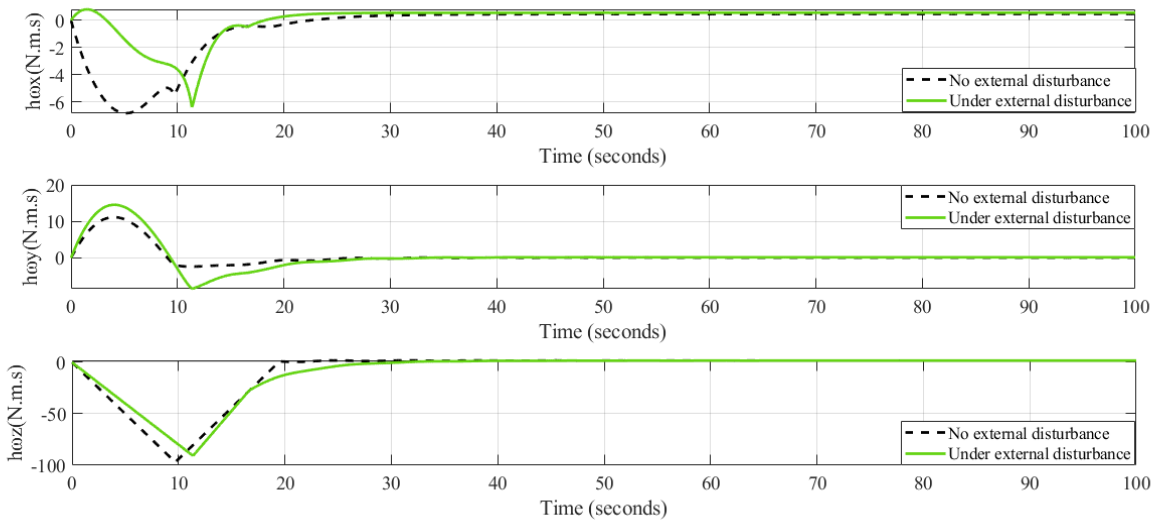

Fig. 10. Reaction wheels angular momentums ($h_{\omega_x}, h_{\omega_y}, h_{\omega_z}$).

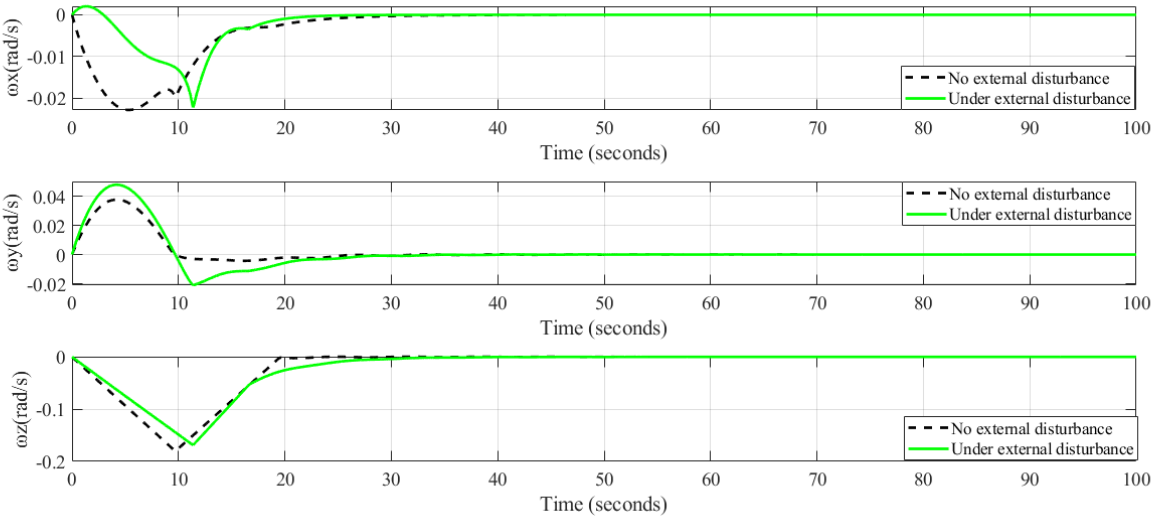

Fig. 11. Flexible satellite angular velocities ($\omega_x, \omega_y, \omega_z$).

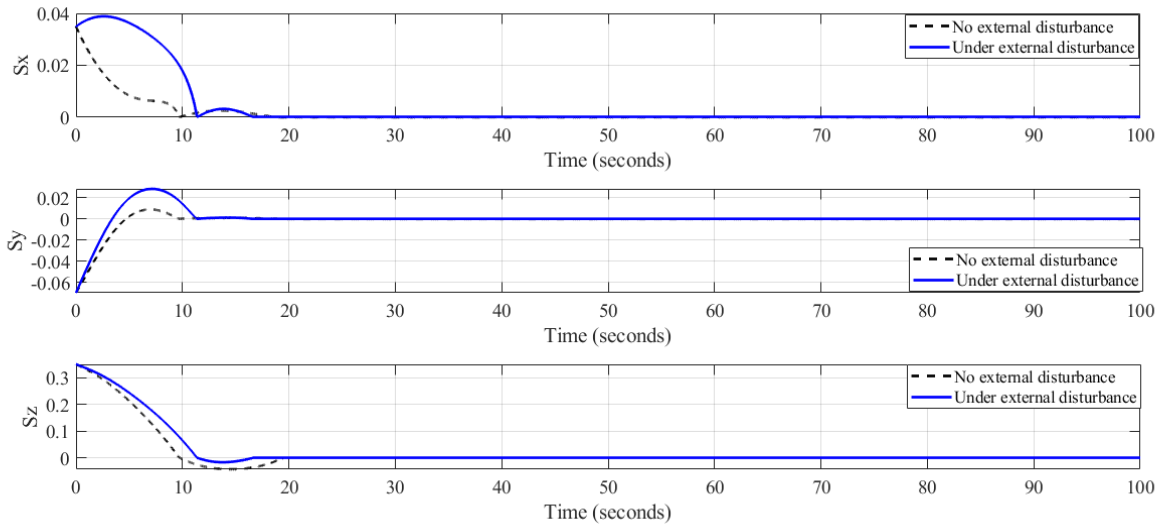

Fig. 12. Sliding surfaces (S_x, S_y, S_z).

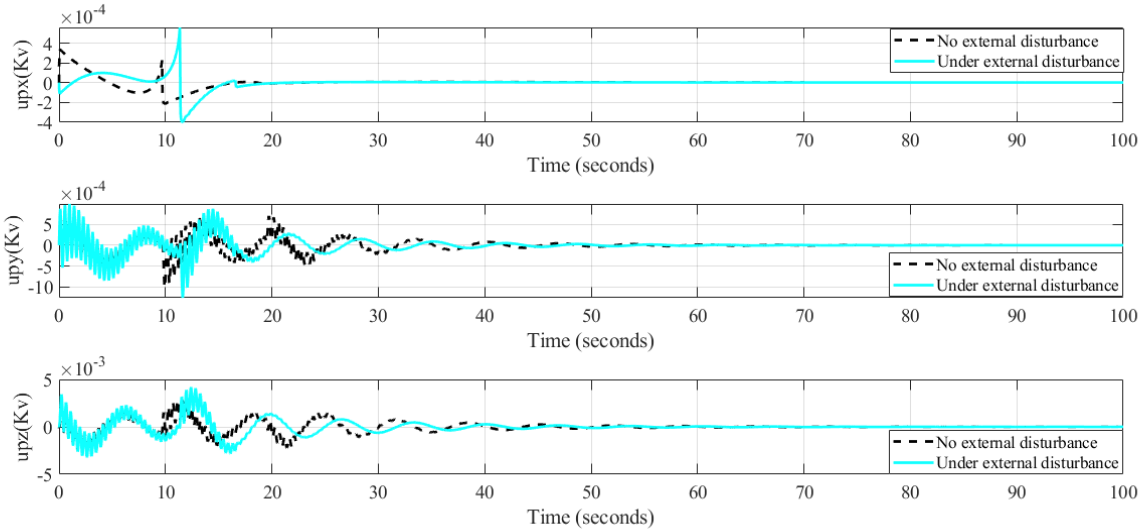

Fig. 13. Piezoelectric voltage inputs ($u_{p_x}, u_{P_y}, u_{P_z}$).

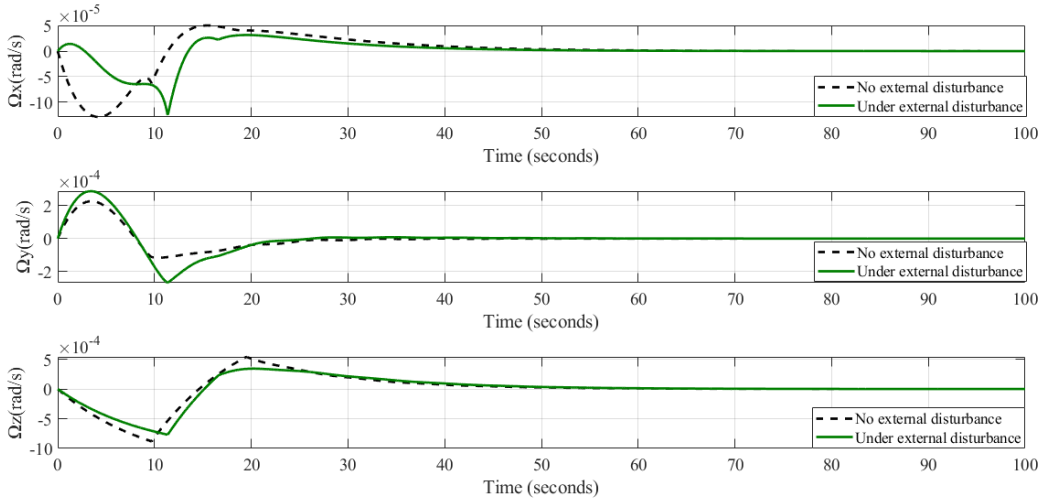

Fig. 14. Reaction wheels motors angular velocities ($\Omega_x, \Omega_y, \Omega_z$) .

Table 3. Hybrid controller characteristics in different methods.

Method name	Euler angles settling time (s)	Max Control effort (N. m)	Max vibration displacement	vibration displacement settling time (s)
No external disturbance	$\phi = 20, \theta = 20, \psi = 22$	10	$\eta_1 = 0.0008, \eta_2 = 0.003, \eta_3 = 0.003$	$\eta_1 = 15, \eta_2 = 50, \eta_3 = 50$
Under external disturbance	$\phi = 25, \theta = 25, \psi = 30$	10	$\eta_1 = 0.0008, \eta_2 = 0.003, \eta_3 = 0.003$	$\eta_1 = 20, \eta_2 = 55, \eta_3 = 55$

Equation (50) and (51) are convergent rate computation, with and without external disturbance respectively.

By assuming two value on the diagram, 80 and 40 the convergence rate is calculated as follows

$$\left|\frac{80-40}{12-8}\right| = \frac{40}{4} = 10 \tag{50}$$

$$\left|\frac{80-40}{14-9}\right| = \frac{40}{5} = 8 \tag{51}$$

The convergent rate by employing the external disturbance is decreased, according to the Fig.5 after employing external disturbance, the settling time increased so it is denoted that the hybrid controller is robust but increasing in settling time is common.

5- 3- Fact Checking

In this subsection, a similar paper is selected to compare with the hybrid controller in this paper [2]. The hybrid controller that is used is merging linear MPC and terminal sliding mode controller. To prove our composite controller feasibility, the selected paper data is used into the composite controller in this paper. The flexible satellite moment of inertia and coupling matrix are given as follows [17].

$$\boldsymbol{J}_0 = \begin{bmatrix} 487 & 15 & -1.2 \\ 14.9 & 177 & -7.3 \\ -1.2 & -7.3 & 404 \end{bmatrix} \tag{52}$$

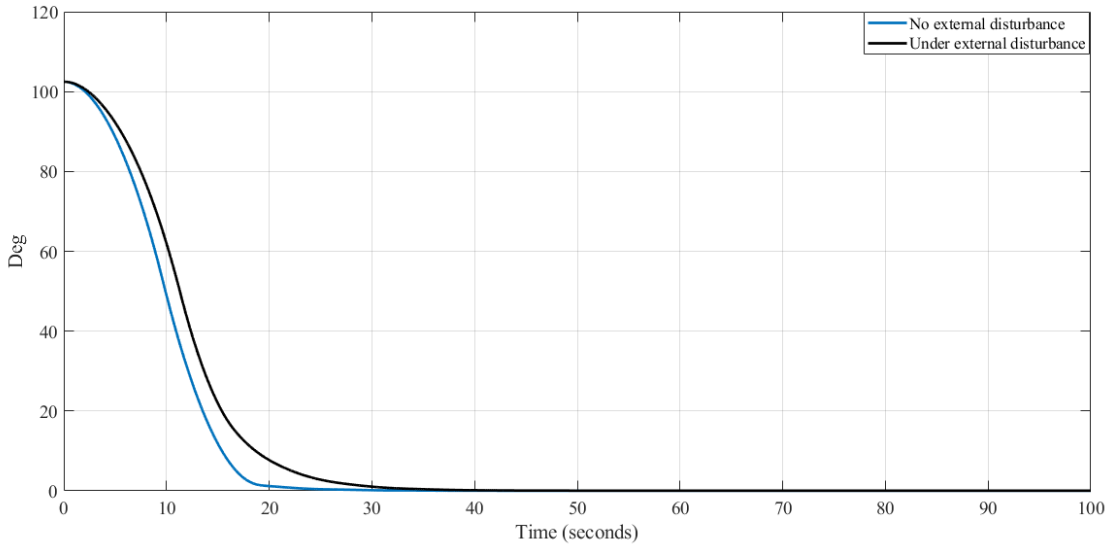

Fig. 15. Euler angles error signals diagram.

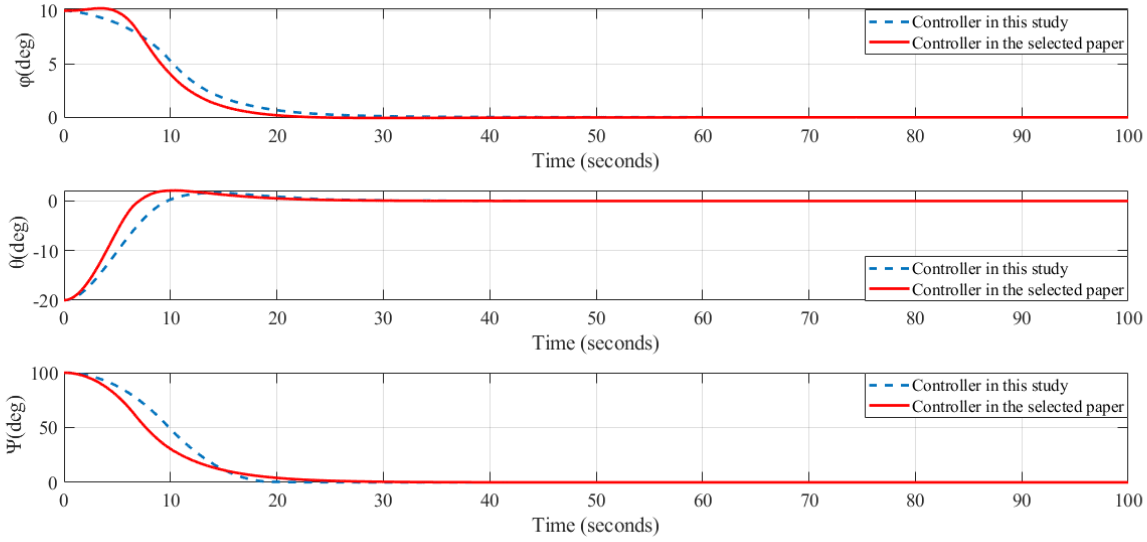

Fig. 16. Flexible satellite Euler angles comparison (ϕ,θ,ψ).

$$\delta = \begin{bmatrix} 1 & 0.1 & 0.1 \\ 0.5 & 0.1 & 0.01 \\ -1 & 0.3 & 0.01 \end{bmatrix} \tag{53}$$

Initial parameters including, gains, prediction horizon and initial angles are the same as Table 1. Fig.16 to 25 are illustrated and compared each other.

Fig.16 is the comparison of the Euler angles of two different methods, and it is understood from the graph that the controller in this study has lower overshoot and undershoot rather than another controller, Fig.17 is the control effort comparison and Fig 18 and 19 are related to satellite angular velocity and angular momentum respectively.Fig.20 and Fig.21 are related to the vibration displacement and velocity respectively, Fig.22 denotes the piezoelectric actuators input control, Fig.23 is Rodiguez parameter, Fig.24 is sliding surfaces and they are converged to zero properly and the last one, Fig.25 is reaction wheels motors angular velocity and they are converged to zero and it means the reaction wheels after completing maneuver are rested.

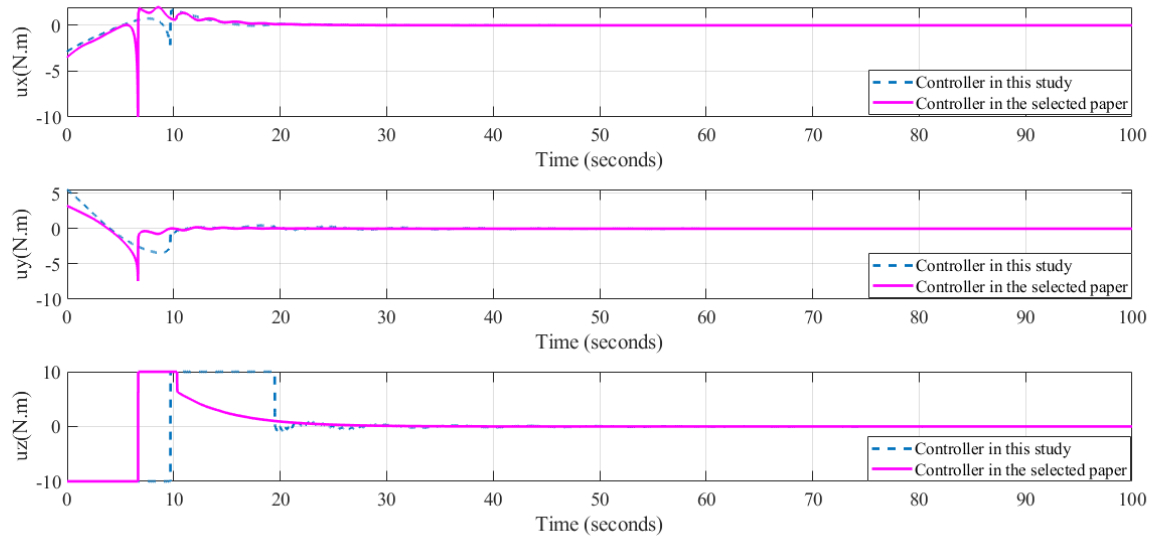

Fig. 17. Control effort signals comparison (u_x, u_y, u_z).

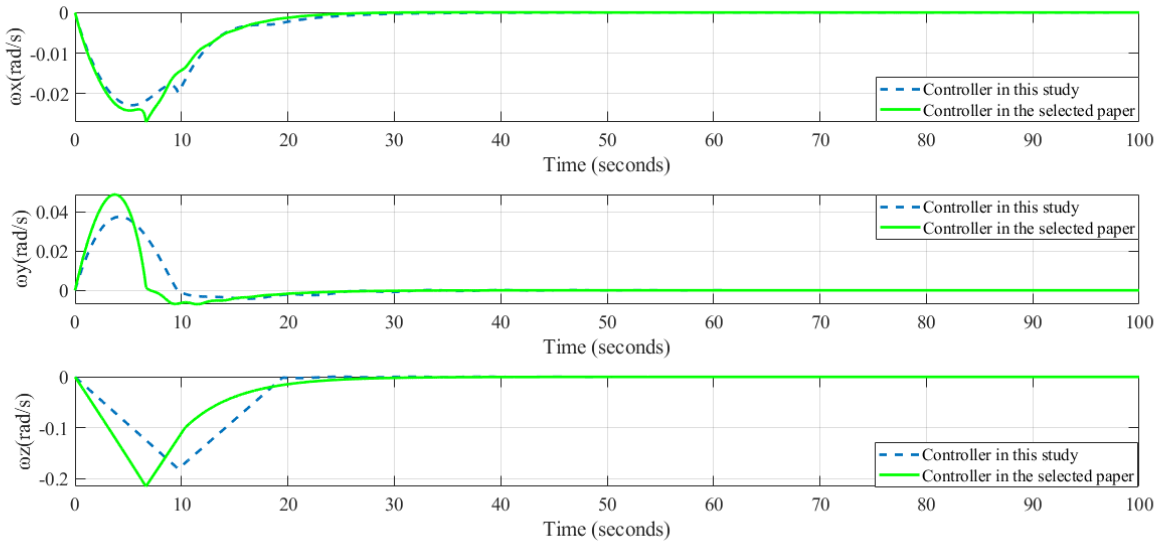

Fig. 18. Flexible satellite angular velocities comparison ($\omega_x, \omega_y, \omega_z$).

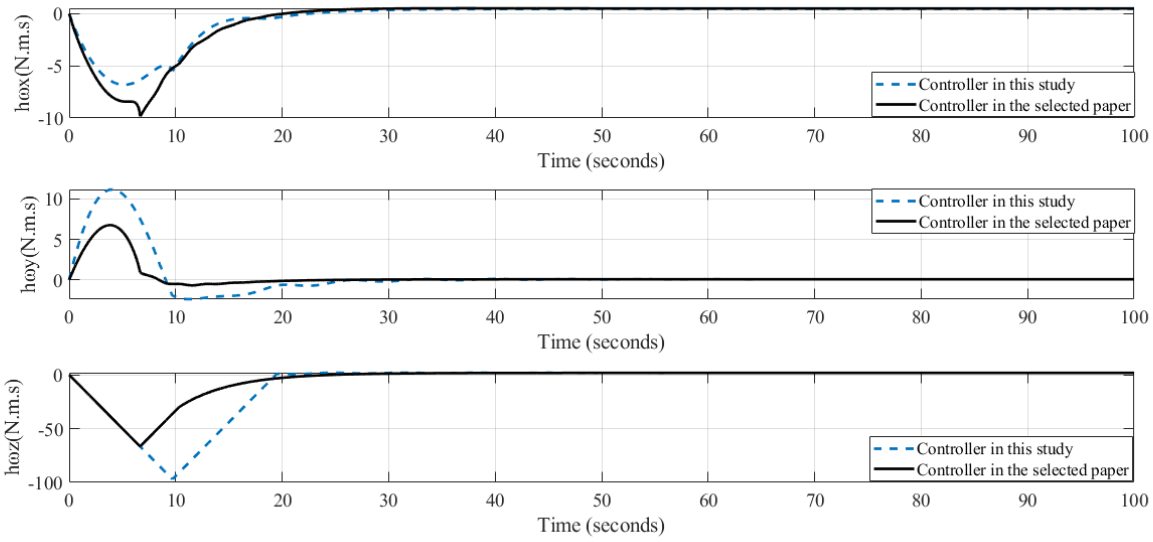

Fig. 19. Satellite angular momentums comparison ($h_{\omega_x}, h_{\omega_y}, h_{\omega_z}$).

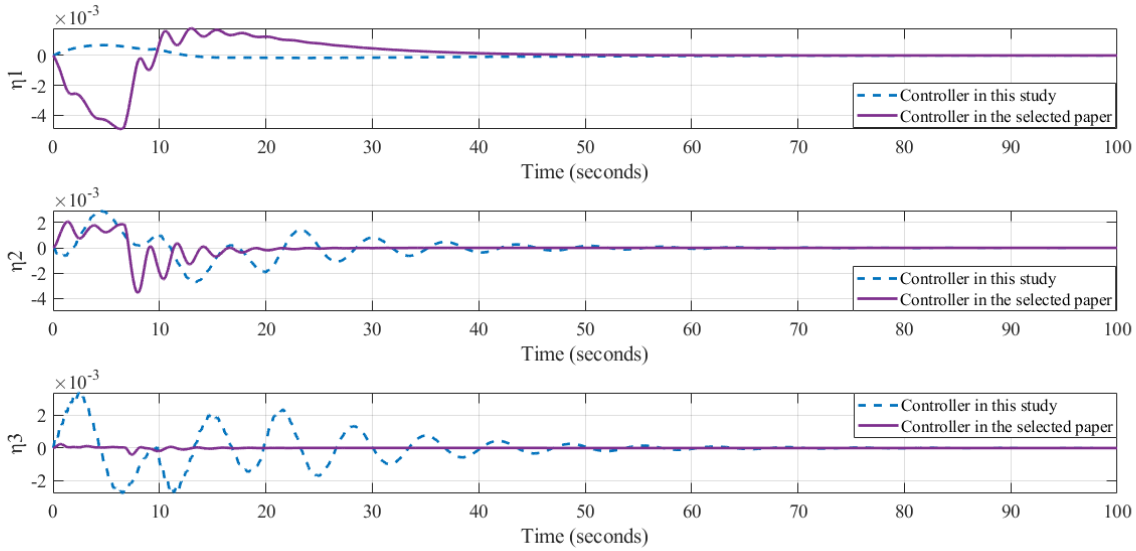

Fig. 20. Vibration displacements comparison (η_1, η_2, η_3).

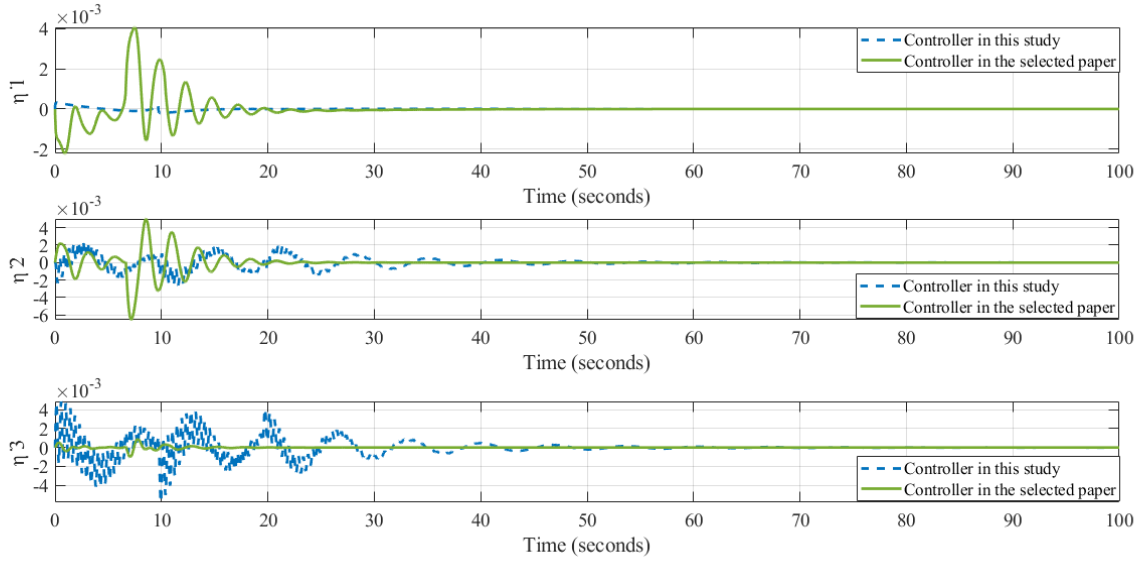

Fig. 21. Vibration velocities comparison ($\dot{\eta}_1, \dot{\eta}_2, \dot{\eta}_3$).

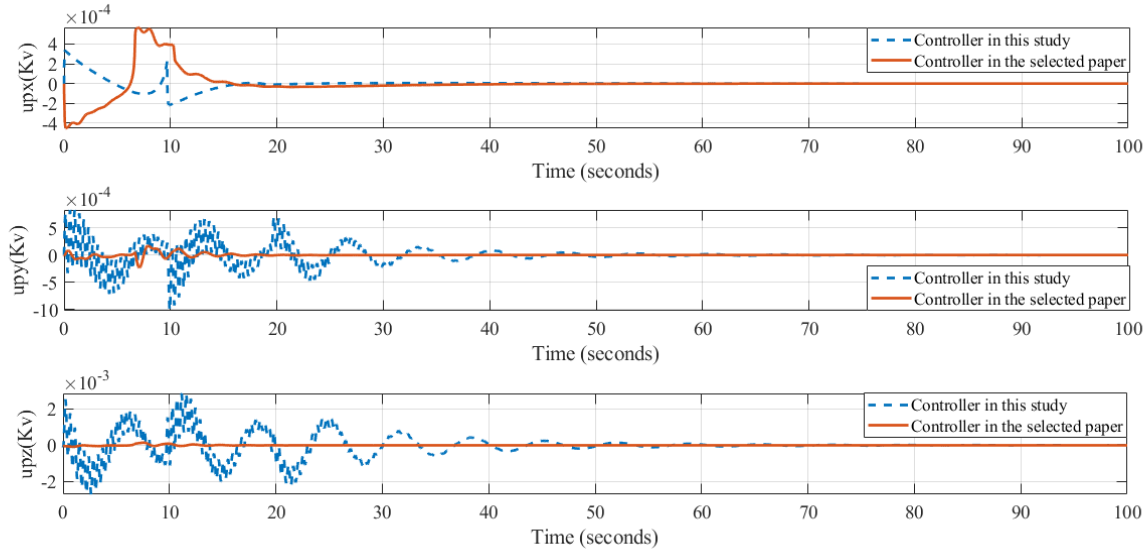

Fig. 22. Piezoelectric voltage inputs comparison ($u_{p_x}, u_{P_y}, u_{P_z}$).

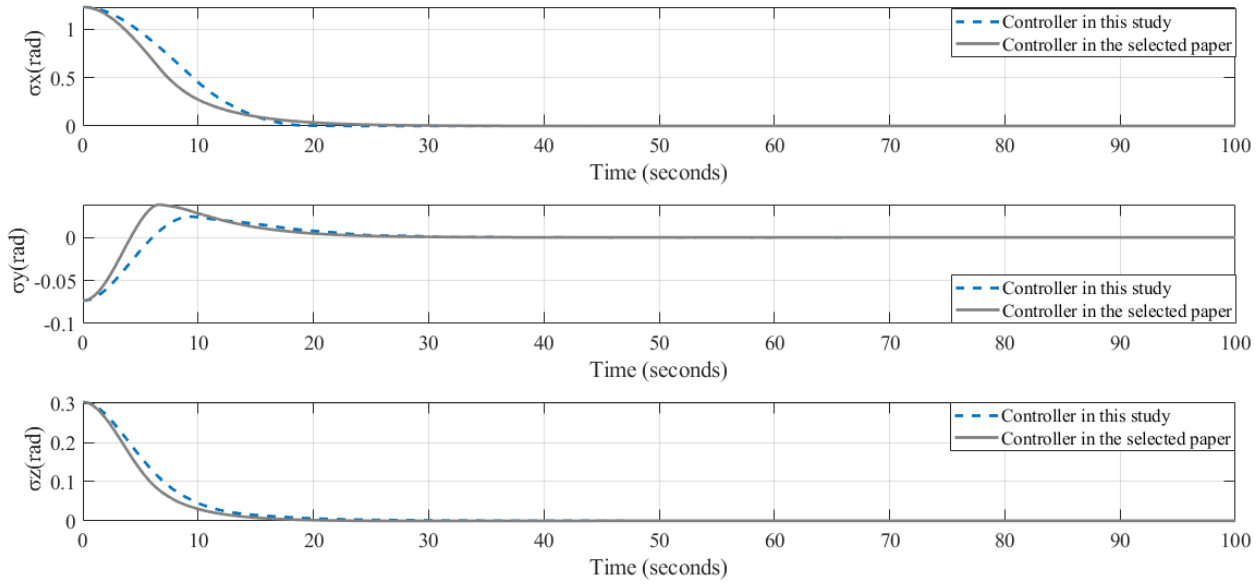

Fig. 23. Modified Rodriguez Parameters comparison ($\sigma_x, \sigma_y, \sigma_z$).

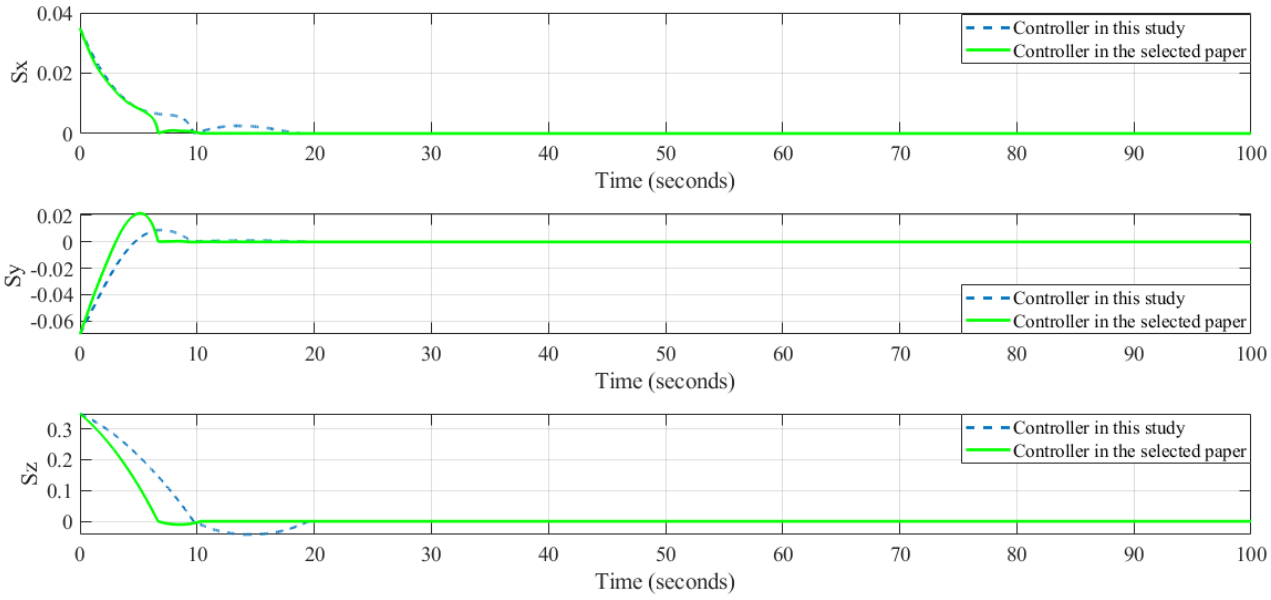

Fig. 24. Sliding surfaces comparison (S_x, S_y, S_z).

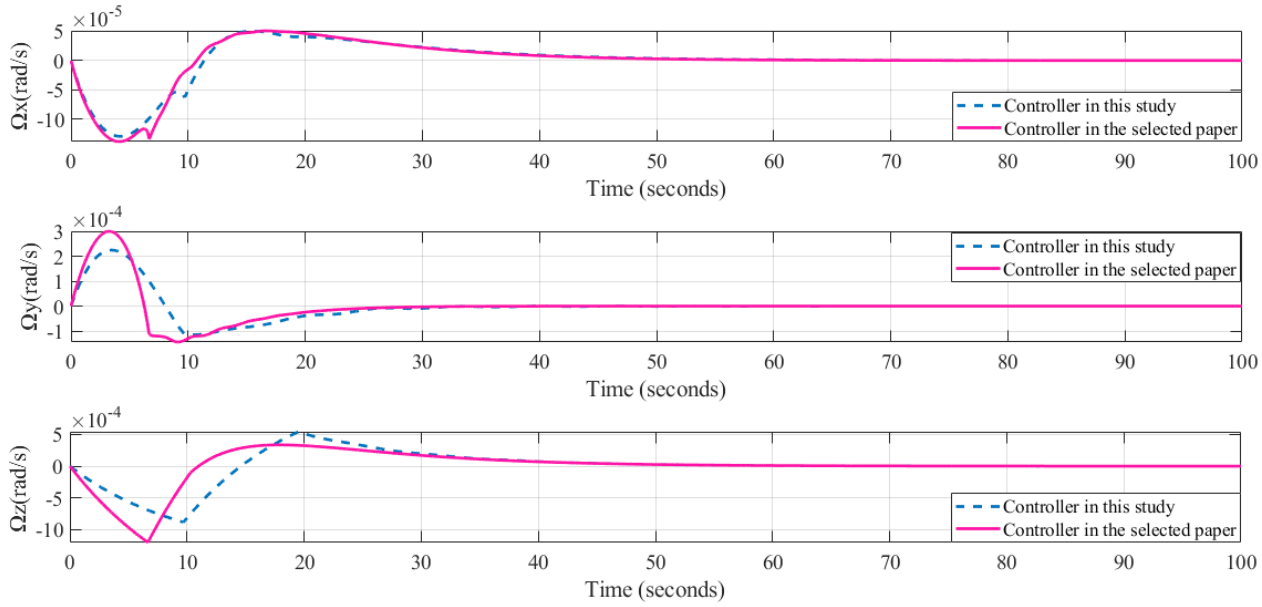

Fig. 25. Reaction wheels motors angular velocities comparison ($\Omega_x, \Omega_y, \Omega_z$).

Table 4. Controllers comparison.

Method name	Euler angles settling time (s)	Max Control effort (N. m)	Max vibration displacement	vibration displacement settling time (s)
Controller in this study	$\phi = 20, \theta = 15, \psi = 20$	10	$\eta_1 = 0.001, \eta_2 = 0.0025, \eta_3 = 0.003$	$\eta_1 = 15, \eta_2 = 50, \eta_3 = 50$
Controller in the selected paper	$\phi = 25, \theta = 20, \psi = 25$	10	$\eta_1 = 0.002, \eta_2 = 0.002, \eta_3 = 0.0005$	$\eta_1 = 40, \eta_2 = 20, \eta_3 = 10$

According to the Table 4, the composite controller in this paper has performed quite well and the Euler angles could reach their setpoints in a shorter time.

6- Conclusion

This paper aims to clarify the effectiveness of the Lyapunov Nonlinear Model Predictive Controller (LNMPC) and its performance when combined with the Anti -Unwinding Sliding Mode Control (AUSMC). The active-set optimization algorithm, known for its speed and accuracy, enhances the usability of this approach, as demonstrated by simulation results. This combination effectively addresses uncertainties and external disturbance, resulting in a longer settling time but still robustness against them. The robustness of the LNMPC is particularly beneficial for managing low-frequency vibrations, which is a significant aspect reflected in the results. Since satellite vibrations typically occur within a low-frequency range, relying solely on LNMPC may not effectively mitigate these vibrations. Therefore, integrating LNMPC with AUSMC proves advantageous, as it leverages the strengths of both controllers.

References

[1] G. Cimini, A. Bemporad, Exact Complexity Certification of Active-Set Methods for Quadratic Programming, IEEE Transactions on Automatic Control, 62(12) (2017) 6094-6109 doi: 10.1109/tac.2017.2696742.

[2] M.M. Maria Khodaverdian, Fault-tolerant model predictive sliding mode control with fixed-timeattitude stabilization and vibration suppression of flexible spacecraft, Elsevier,Journal of Space Safety Engineering,139(2023)doi: 10.1016/j.ast.2023.108381.

[3] M.K.M. Malekzadeh, Attitude stabilization of spacecraft simulator based on modifiedconstrained feedback linearization model predictive control, IET Control Theory & Applications, 17(8) (2023) 15 953-967 doi: 10.1049/cth2.12429.

[4] U.U.V.K.c. Avishai Weiss, Stefano Di Cairano, Station keeping and momentum management of low-thrust satellitesusing MPC, Elsevier,Aerospace Science and Technology, (2018) doi: 10.1016/j.ast.2018.02.014.

[5] R.A.J.C. Paulo Henrique dos Santos Satellite attitude control using extended model predictivecontrol(EMPC) underactuatorfailures,Elsevier,(2024)doi: 10.1016/j.asr.2024.05.010.

[6] N.A. MohammadAmin AlandiHallaj, Multiple-horizon multiple-model predictive control of electromagnetictethered satellite system, Elsevier,Acta Astronautica, (2019) doi: 10.1016/j.actaastro.2018.11.003.

[7] A.M.H. M. Amin Alandihallaj, Jan Thoemel, Model predictive control-based satellite docking control for on-orbitrefueling mission, Elsevier,Journal of Space Safety Engineering, (2025) doi: 10.1016/j.jsse.2025.03.007.

[8] K.V.L. Xiaohua Zhang, Zhengliang Lu,Xiang Zhang,Wenhe Liao,W.S. Lim, Piece-wise affine MPC-based attitude control for a CubeSat duringorbital manoeuvres, Elsevier,Aerospace Science and Technology, (2021) doi: 10.1016/j.ast.2021.106997.

[9] Y.H. Yihong Zhou, Keck-Voon Ling,Feng Ding, Hybrid two-stage identification-based nonlinearMPC strategy for satellite attitude control, IEEE, (2025) doi: 10.1109/TAES.2025.3543466.

[10] M.U.N. SYED MUHAMMAD AMRR, ATIF IQBAL, An Event-Triggered Robust Attitude Control ofFlexible Spacecraft With Modified RodriguesParameters Under Limited Communication, IEEE, (2019) doi: 10.1109/ACCESS.2019.2927616 .

[11] M.A.M.M.A. Ariaei, Active Fractional-Order Sliding Mode Control of FlexibleSpacecraft Under Actuators Saturation, Elsevier, (2022).

[12] M.A.M.M.A. Ariaei, Active Fractional-Order Sliding Mode Control of FlexibleSpacecraft Under Actuators Saturation, Journal of Sound and Vibration, 535 (2022) 13.

[13] Q. Hu, Sliding mode maneuvering control and activevibration damping of three-axis stabilized flexiblespacecraft with actuator dynamics, Springer, (2008) 22 doi: 10.1007/s11071-007-9274-6.

[14] D.J.P. G.A. Andrade, J.D. A´ lvarez,M. Berenguel, A practical NMPC with robustness of stability applied todistributed solar power plants, Elsevier, (2013) doi: 10.1016/j.solener.2013.02.013.

[15] A.-G.W. Rui-Qi Dong, Ying Zhang,Guang-Ren Duan, Anti-unwinding sliding mode attitude control via two modifiedRodrigues parameter sets for spacecraft, Elsevier, (2021) doi: 10.1016/j.automatica.2021.109642.

[16] C.Z.G.M.Y.S. , C. Li, Prescribed performance adaptive attitude tracking controlfor flexible spacecraft with active vibration suppression, Springer, (2019) 18 doi: 10.1007/s11071-019-04894-x .

[17] L.C.B.X.M. Golestani, Robust fixed-time attitude stabilization control of flexiblespacecraft with actuator uncertainty, Springer, (2020) 15 doi: 10.1007/s11071-020-05596-5.

HOW TO CITE THIS ARTICLE

M. Salehipour, M. Malekzadeh, M. Mortazavi, M. Sayanjali, Hybrid Nonlinear Model Predictive Control of a Flexible Satellite, AUT J. Mech Eng., 10(2) (2026) 211-230.

DOI: 10.22060/ajme.2025.24218.6184